Boundary conditions for equilibrating incommensurate periodic patterns

Hiroto Ogawa and Nariya Uchida
Department of Physics, Tohoku University, Sendai 980-8578, Japan
(Received 23 May 2005; published 15 November 2005)

Simulation of periodic patterns often suffer from artifacts due to incommensurability of the intrinsic length scale and the system size. We introduce a simple numerical scheme to avoid this problem in finding equilibrium domain morphologies from a Ginzburg-Landau-type free energy. In this scheme, the boundary values are determined only by the local equilibrium condition at the adjacent bulk sites. The scheme is especially advantageous in equilibrating patterns that have two or more characteristic lengths. We demonstrate it using a model of lamellar-lamellar coexistence in block copolymer blends.

DOI: 10.1103/PhysRevE.72.056707 PACS number(s): 02.70.−c, 61.20.Ja, 61.25.Hq

I. INTRODUCTION

Field models are widely used in mesoscopic description of condensed matter. Numerical minimization of Ginzburg-Landau free energy functionals is often useful in finding the equilibrium structures in the ordered phases, such as those in liquid crystals and block copolymers. Many of the mesophases exhibit periodic domain structures, equilibration of which requires efficient numerical schemes. For instance, global ordering through the ragged energy landscape can be accelerated by simulated annealing [1], incorporating hydrodynamic flow [2] or artificial inertial terms in the Langevin equation [3]. Another, and crucial problem in simulating periodic domain structures is the choice of boundary condition. The periodic boundary condition is preferred to the Dirichlet or Neumann boundary conditions because it retains the translational invariance. However, even the periodic boundary condition must be used with care when the size of the simulation box is not commensurate with the intrinsic period of the pattern, which is quite a general case. Equilibrium morphologies in such a case can be very different from those in a bulk system; an example for a block copolymer system is given in Ref. [4]. To minimize the finite-size effect, we must choose the box size equal to or a multiple of the intrinsic length scale, which is not known beforehand in most cases. There are some clever algorithms that adjust the box size to the intrinsic period [5–8]. They have been developed in the context of molecular dynamics (MD) or MD Monte Carlo hybrid simulations. For example, Parrinello and Rahman [6] extended a constant-pressure MD algorithm [5] by regarding both the box size and shape as dynamical variables obeying Newton's second law of motion. Originally developed for simulation of crystalline structures, it has been successfully applied also to polymeric mesophases [9]. However, these box-size adjusting methods are not sufficient when the system has two or more intrinsic length scales that are not commensurate with each other. For example, consider the chiral smectic-C phase of a liquid crystal. It has two characteristic periods along the layer normal, namely the layer thickness and the twisting pitch. In general, they are not commensurate with each other, and hence cannot be commensurate with the box dimension at the same time. In this way, if there are two or more characteristic periods in the same direction, the box size is incommensurate with at least one of the intrinsic length scales.

In the present paper, we introduce a simple boundary condition that avoids the above-mentioned problem. In this scheme, the boundary values are determined only by the local equilibrium condition at the bulk sites adjacent to the boundary. Therefore we call our new boundary condition "local equilibrium boundary condition." In this scheme, we update the boundary values to reduce the deviation from local equilibrium at the nearest bulk sites. Thus, equilibration at the boundary proceeds in company with equilibration in the bulk.

The organization of this paper is as follows. In Sec. II, we introduce the local equilibrium boundary condition. In Sec. III, the scheme is applied to equilibrium patterns of block copolymer blends in lamellar-lamellar phase coexistence. In Sec. IV we discuss the results and advantage of the present scheme over conventional boundary conditions. We conclude in Sec. V.

II. LOCAL EQUILIBRIUM BOUNDARY CONDITION

In this section, we explain the concept and implementation of the local equilibrium boundary condition using simple field models to find the equilibrium morphology. We consider a system described by an order parameter $\psi(\mathbf{r},t)$ with a free energy $F[\psi(\mathbf{r},t)]$ containing only local interactions (given in terms of gradient expansion). The task is to minimize the free energy by numerically solving a simple dynamic equation for the order parameter. Since our purpose is to obtain the equilibrium morphology, the dynamic equation is not required to describe the realistic dynamical processes and can be chosen with some arbitrariness, as long as it decreases the free energy in time and does not violate conservation laws. First we consider the nonconserved case, and assume the dynamic equation

$$\frac{\partial \psi}{\partial t} = -\frac{\delta F}{\delta \psi}. \tag{1}$$

To be concrete, we use the free energy

$$F = \int d\mathbf{r}\left(\frac{A}{2}\psi^2 + \frac{B}{4}\psi^4 + \frac{C}{2}(\nabla\psi)^2\right), \tag{2}$$

when necessary, for which Eq. (1) becomes the Allen-Cahn equation [10]. In numerical simulation, the right-hand side of Eq. (1) is discretized in the form

$$-\left\langle \frac{\delta F}{\delta \psi} \right\rangle_i = -A\hat{\psi}_i - B\hat{\psi}_i^3 + \frac{C}{(\Delta x)^2}\sum_j L_{ij}\hat{\psi}_j, \tag{3}$$

where $\langle\ \rangle$ is the discretization operator, i and j are site indices, $\hat{\psi}_i$ is the value of ψ at i, Δx the grid size, and L_{ij} the coefficient matrix of the discretized Laplacian. On the d-dimensional hypercubic lattice, for example, we can set

$$L_{ij}\begin{cases} =-2d & \text{if } i=j, \\ =1 & \text{if } i \text{ and } j \text{ are nearest neighbors}, \\ =0 & \text{otherwise}. \end{cases} \tag{4}$$

The time-discretized dynamic equation in the Euler scheme is

$$\frac{\hat{\psi}_i(t+1)-\hat{\psi}_i(t)}{\Delta t} = -\left\langle \frac{\delta F}{\delta \psi} \right\rangle_i (t), \tag{5}$$

where Δt is the time step. The equilibration procedure is to solve it under an appropriate boundary condition.

In the fully equilibrated state, the local equilibrium condition $\langle \delta F/\delta\psi\rangle = 0$ holds at any bulk site, while at boundary sites we cannot evaluate $\langle \delta F/\delta\psi\rangle$ as it contains spatial derivatives of the order parameter. To determine the boundary value, we shall focus on any bulk site a which is adjacent to a boundary site b. Our idea is to update the boundary value $\hat{\psi}_b$ towards the local equilibrium condition at the adjacent site,

$$\left\langle \frac{\delta F}{\delta \psi} \right\rangle_a = 0. \tag{6}$$

This idea is implemented by the following dynamic equation, which reduces $\langle \delta F/\delta\psi\rangle_i$ in time,

$$\frac{\partial \hat{\psi}_b}{\partial t} = -\frac{\partial}{\partial \hat{\psi}_b}\sum_a W\left(\left\langle \frac{\delta F}{\delta \psi} \right\rangle_a\right). \tag{7}$$

Here, the sum is taken over the bulk sites adjacent to b, and $W(x)$ is a potential function that has only one minimum at $x=0$. The simplest choice would be the parabola,

$$W(x) = \frac{w_0}{2}x^2.$$

The curvature w_0 must be chosen so that equilibration proceeds simultaneously at the boundary and in the bulk. If w_0 is too large, the local equilibrium condition (6) is satisified instantaneously, which means that $\hat{\psi}_i$ is frozen [as it obeys Eq. (5)]. If w_0 is too small, then $\hat{\psi}_b$ will not change much from the initial value until the bulk equilibrates.

It is straightforward to extend the above scheme to a conserved system, which is described by the dynamic equation

$$\frac{\partial \psi}{\partial t} = \nabla^2 \frac{\delta F}{\delta \psi}. \tag{8}$$

We approach the stationarity condition at the adjacent bulk site,

$$\left\langle \nabla^2 \frac{\delta F}{\delta \psi} \right\rangle_a = 0, \tag{9}$$

by solving the dynamic equation for the boundary values,

$$\frac{\partial \hat{\psi}_b}{\partial t} = -\frac{\partial}{\partial \hat{\psi}_b}\sum_a W\left(\left\langle \nabla^2 \frac{\delta F}{\delta \psi} \right\rangle_a\right). \tag{10}$$

We note that the local equilibrium condition for a conserved system is given by $\mathbf{j} \equiv -\boldsymbol{\nabla}(\delta F/\delta\psi) = \mathbf{0}$ and is stronger than the stationarity condition $\nabla^2(\delta F/\delta\psi) = 0$. However, decrease of the current $\mathbf{j}$ in the bulk together with stationarity at the boundary naturally ensures the decrease of $\mathbf{j}$ at the boundary. For simplicity, we call Eq. (10) the local equilibrium condition.

Here we have a remark on the definition of the boundary sites. Let us consider a hypercubic lattice of size N^d, whose sites are located at $\mathbf{r} = (r_1\Delta x, r_2\Delta x, \ldots, r_d\Delta x)$ where $r_s = 1, 2, \ldots, N$ $(s = 1, 2, \ldots, d)$. Let us call a pair of sites i and j are in the nth shell of each other, when they satisfy

$$\max_s |r_{s,i} - r_{s,j}| = n. \tag{11}$$

For the model free energy (2) and the Laplacian (4), calculation of $\langle \delta F/\delta\psi\rangle_i$ requires $\nabla^2\psi$ at the site i, which involves only the first shell of i. Therefore, for the nonconserved case, the boundary sites are simply the sites in the outermost layer of the lattice; at least one of the site coordinates x_s equals 1 or N. On the other hand, for the conserved case, calculation of $\langle \nabla^2 \delta F/\delta\psi\rangle_i$ requires a fourth-order derivative, which involves both the first and second shells of i. Therefore, we define the boundary sites as the sites in the first and second outermost layers of the lattice; at least one of the site coordinates r_s equals 1, 2, $N-1$, or N. In this way, our definition of the boundary sites depends on the model free energy, discretization scheme, and the dynamic equation.

Now we comment on the range of applicability of the proposed scheme. As mentioned above, the potential function $W(x)$ and its curvature must be chosen carefully to avoid freezing of the boundary values in the early stage of equilibration. In general, W can be a functional containing the gradients of $\delta F/\delta\psi$ (nonconserved case) or $\nabla^2 \delta F/\delta\psi$ (conserved case). Sometimes we find it better to minimize the square of $\langle \boldsymbol{\nabla}\delta F/\delta\psi\rangle_a$ than the square of $\langle \delta F/\delta\psi\rangle_a$, because the latter directly leads to vanishing of $\langle \delta F/\delta\psi\rangle_a$ and easily stops relaxation at the boundary. However, we do not have a general prescription at the moment and limit ourselves to a simplest possible choice.

Finally we should mention a restriction on the initial condition. Our scheme with the conventional bulk dynamic equation such as (1) or (8) is not sufficient to obtain true equilibrium patterns from disordered initial conditions. In fact, the initial configuration must be well ordered in that it is free from defects or contains only a small amount of defects. This is because the motion of defects is driven by deviation from the local equilibrium condition. The deviation at the boundary decays to zero exponentially fast according to Eq. (7) or Eq. (10), while the bulk dynamics (1) or (8) leads to power-law-type slow coarsening of defects. Therefore, de-

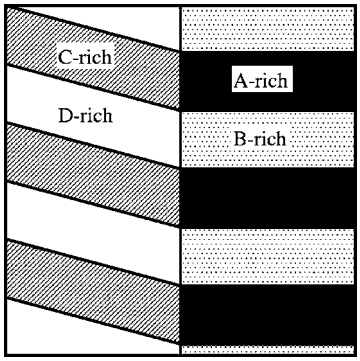

FIG. 1. A schematic domain morphology of coexisting lamellar phases. Layers with different thicknesses are joined by making a finite angle between them.

fects are trapped at the boundary before they can annihilate in the bulk. In order to obtain a defect-free equilibrium pattern from an arbitrary initial condition, we must modify the bulk dynamic equation and avoid trapping by local minima of the free energy. Such accelerated equilibration schemes for periodic patterns have been proposed in various contexts [1–3]. We could attempt to combine these methods for the bulk and our new boundary scheme, which is a subject of future work. In the present paper, we limit ourselves to a demonstration of our new boundary condition with a conventional bulk dynamic equation. This means that we must choose an initial configuration sufficiently close to the equilibrium one.

III. SIMULATION OF BLOCK COPOLYMER BLENDS

In this section, we test the local equilibrium boundary condition in a two-dimensional simulation of diblock copolymer melts. We focus on the lamellar-lamellar phase coexistence in a mixture of *AB* and *CD* symmetric diblock copolymers. The chain lengths of *AB* polymer and *CD* polymer are different. This results from a macrophase separation into *AB*-rich and *CD*-rich domains, each of which are microphase separated into $A(C)$-rich and $B(D)$-rich layers (respectively). In equilibrium, the *AB*-rich and *CD*-rich lamellae have different layer widths due to the different chain length, and make a certain angle to each other so that the *A*-rich and *C*-rich layers are smoothly connected at the phase boundary; see Fig. 1. How can we numerically reproduce this domain morphology? It is clear that the pattern is not compatible with the periodic boundary condition, unless there holds a special lucky relation between the system size, the two layer thicknesses, and the angle between the layers. Therefore, the lamellar-lamellar coexistence provides an ideal test case for our local equilibrium boundary condition. We compare it with the periodic boundary condition by examining the stability of ordered phase. For this purpose, we can use the initial condition close to the equilibrium configuration.

We use a phenomenological Ginzburg-Landau model adopted by Ohta *et al.* [13]. Below we will briefly summarize their model. The order parameters are $\phi_0=\delta\phi_A+\delta\phi_B$, $\phi_1=\phi_A-\phi_B$, and $\phi_2=\phi_C-\phi_D$, where ϕ_K is the volume fraction of K segment and $\delta\phi_K=\phi_K-\bar{\phi}_K$ is its spatial fluctuation $(K=A,B,C,D)$. The incompressibility condition $\Sigma_K\phi_K=1$ is assumed. The free energy is a sum of local and long-range parts,

$$F = F_{\text{local}}[\phi_0,\phi_1,\phi_2] + F_{\text{long}}[\phi_1,\phi_2]. \tag{12}$$

The local part is given in the form

$$F_{\text{local}} = \int d\mathbf{r}\left[\sum_{K=0,1,2}\left(g_K(\phi_K)+\frac{C_K}{2}(\nabla\phi_K)^2\right) - \frac{B_0}{2}\phi_1\phi_2 - \frac{B_1}{2}\phi_0\phi_1^2 + \frac{B_2}{2}\phi_0\phi_2^2\right], \tag{13}$$

where B_i and C_i are constants and $g_K(x)$ is a double-well function. Instead of the conventional polynomial form $g_K(x)=-x^2/2+x^4/4$, we choose the form

$$g_K(x) = -A_K\ln(\cosh x) + \frac{x^2}{2}, \tag{14}$$

which enhances numerical stability [11].

The long-range repulsive interaction between the same species, which is an entropic effect due to the *A*-*B* and *C*-*D* bondings, is given by

$$F_{\text{long}} = \sum_{K=1,2}\frac{\alpha_K}{2}\int d\mathbf{r}\int d\mathbf{r}'\,\delta\phi_K(\mathbf{r})G(\mathbf{r}-\mathbf{r}')\delta\phi_K(\mathbf{r}'), \tag{15}$$

where the coefficient α_K is proportional to N_K^{-2} (see Ref. [13]), N_1 and N_2 being the chain length of *AB* and *CD* copolymers (respectively), and the kernel $G(\mathbf{r})$ is defined by $-\nabla^2 G(\mathbf{r})=\delta(\mathbf{r})$. The dynamic equations are of conserved type and read

$$\frac{\partial\phi_K}{\partial t} = \nabla^2\frac{\delta F}{\delta\phi_K} \quad (K=0,1,2). \tag{16}$$

Using the property of $G(\mathbf{r})$ mentioned above, the equations for ϕ_1 and ϕ_2 can be rewritten as

$$\frac{\partial\phi_K}{\partial t} = \nabla^2\frac{\delta F_{\text{local}}}{\delta\phi_K} - \alpha_K(\phi_K-\bar{\phi}_K). \tag{17}$$

Thus, although the free energy contains long-range interaction, the dynamic equations are completely local and contains only spatial derivatives, which is a requisite for implementing our local boundary conditon. We use its dynamic version, Eq. (10), with ψ replaced by ϕ_K and the potential function for each component,

$$W_K(x) = \frac{w_K}{2}x^2 \quad (K=0,1,2). \tag{18}$$

Now we define some terminology to avoid confusion. We use "boundary" for the first and second outermost sites of the simulation box and "interface" for the domain wall between *AB*-rich and *CD*-rich regions. Assuming sine-wave profiles for the lamellae and a sigmoidal profile for the interface, we estimated the amplitudes, layer thickness, and interfacial

thickness of the equilibrium morphology; see the Appendix for details. With these we constructed a trial equilibrium pattern, which we chose to be our initial condition,

$$\phi_0(\mathbf{r}) = \Phi_0 \tanh(kx),$$

$$\phi_1(\mathbf{r}) = \Phi_1 + \Delta_1 \tanh(kx)\cos(\mathbf{q}_1 \cdot \mathbf{r} + \theta_1),$$

$$\phi_2(\mathbf{r}) = \Phi_2 + \Delta_2 \tanh(kx)\cos(\mathbf{q}_2 \cdot \mathbf{r} + \theta_2), \tag{19}$$

where we assumed the interface is located at $x=0$. In order to lower the interfacial energy, the cross-sectional profiles of the two phases at $x=0$ must match (see Fig. 1). This gives the relations $\theta_1=\theta_2$ and $q_{1y}=q_{2y}\equiv Q$, the latter leading to $q_{Kx}=\pm\sqrt{q_K^2-Q^2}$ $(K=1,2)$. Since the equilibrium wave numbers $|\mathbf{q}_1|$ and $|\mathbf{q}_2|$ are known, the value of Q can be determined by the angle

$$\gamma = \arctan\left|\frac{q_{1x}}{q_{1y}}\right|, \tag{20}$$

which we regard as an adjustable parameter in our initial condition.

The parameter values we used are $A_0=1.3$, $A_1=1.0001$, $A_2=1.1$, $B_0=0.1$, $B_1=0.085$, $B_2=0.09$, $C_0=C_1=C_2=0.5$, $\alpha_1=0.000\,95$, and $\alpha_2=0.019$. The angle γ is set to 50° unless stated otherwise. The grid size is $\Delta x=1$, and the time step is $\Delta t=0.1$. The parameters for the local equilibrium boundary condition are chosen to be $w_0=w_1=w_2=2$. These values are chosen by the following consideration. First, A_0 determines the amplitude ϕ_0 of macrophase separation into the *AB*-rich $(\phi_0>0)$ and *CD*-rich $(\phi_0<0)$ phases. We assumed strong segregation, $|\phi_0|\simeq 1$. The thickness of the interface is estimated from C_0. For each macrophase, we fixed the amplitudes ϕ_K $(K=1,2)$ of the lamellae in terms of A_K and B_K. The amplitudes are chosen small enough, which corresponds to weak segregation. The coupling B_1 (B_2) induces microphase separation in the *AB*-rich (*CD*-rich) domain, in which the amplitude of $\phi_1(\phi_2)$ must be larger than the other (respectively). The coupling B_0 describes the attraction of *A*-*C* and *B*-*D*, because of which the *AB* and *CD* lamellae tend to fit each other at the interface. Once given the equilibrium amplitudes of lamellae, we can control the layer thicknesses through α_K and C_K. Especially, from the value of α_K, the ratio of the two chain lengths can be calculated as $N_1:N_2=\sqrt{0.019}:\sqrt{0.000\,95}=2\sqrt{5}:1$. For more details, see the Appendix and also Ref. [13]. We also found that the system is close to equilibrium when the angle γ is about 50°. For other values of γ we tested, the system was trapped in local minima of the free energy, as explained in the next section.

IV. RESULT AND DISCUSSION

In Fig. 2, we show the snapshots of the order parameters at $t=0$, 100, 500, and 1000. The results for the local equilibrium and the periodic boundary conditions are shown in the left-hand and right-hand columns, respectively. In each snapshot, $\phi_1(\mathbf{r})$ is plotted in the *AB*-rich domain [where $\phi_0(\mathbf{r})>0$], while $\phi_2(\mathbf{r})$ is plotted in the *CD*-rich domain. With the periodic boundary condition, the lamellae get deformed near the boundary. This is to smoothly connect the domains at the two ends, at the cost of elastic bending energy. On the other hand, the local equilibrium boundary condition induces only a slight deformation of the lamellae. Thus the new boundary

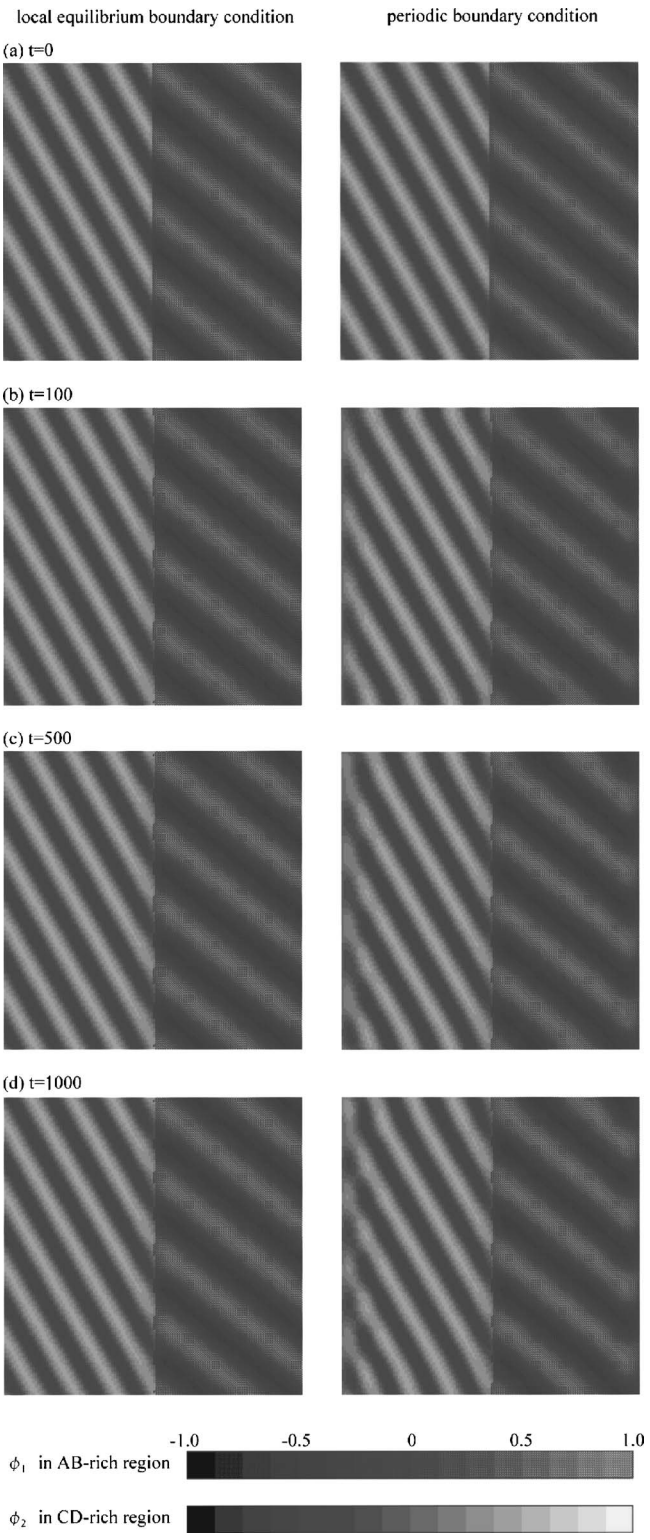

FIG. 2. Time evolution of the coexisting lamellar patterns. Snapshots at (a) $t=0$, (b) $t=100$, (c) $t=500$, and (d) $t=1000$. The left-hand and right-hand columns show the result for the local equilibrium and periodic boundary condition, respectively.

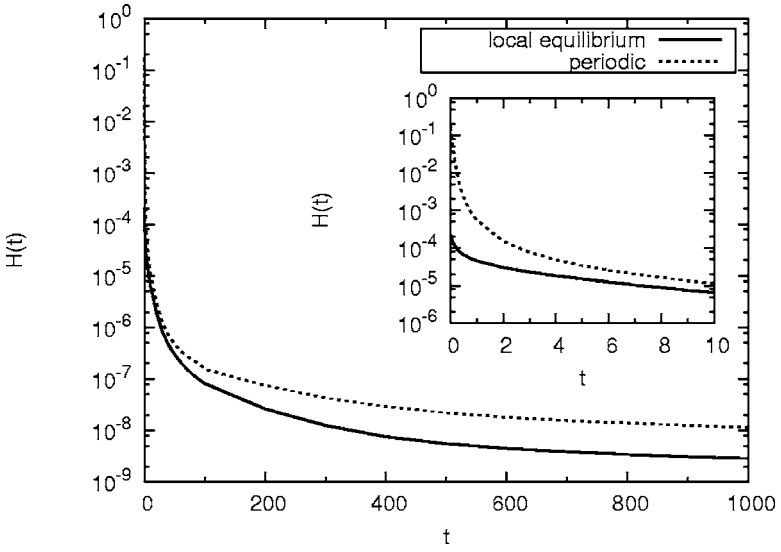

FIG. 3. Decay of the mean-square relaxation rate $H(t)$ for the local equilibrium and periodic boundary conditions. The solid line (local equilibrium) is always below the dotted line (periodic). Inset, relaxation in the early stage.

condition causes less finite-size effects compared to the periodic one, not only in the morphological sense but also in lowering the free energy.

To further compare the two boundary conditions (the local equilibrium and the periodic), we measured the mean-square relaxation rate

$$H(t) = \sum_{K=0,1,2} \overline{\left(\frac{\partial \phi_K}{\partial t}\right)^2} = \sum_{K=0,1,2} \overline{\left(\nabla^2 \frac{\delta F}{\delta \phi_K}\right)^2}, \qquad (21)$$

which quantifies the deviation from equilibrium. We plot $H(t)$ in Fig. 3. We see that $H(t)$ for the local equilibrium condition is always smaller than that for the periodic boundary condition. We note that the difference between $H(t)$ for the two boundary conditions is largest at $t=0$ (see the inset of Fig. 3). This difference is due to the mismatch of the domains at the two ends, and is reduced mainly in the early stage. In the final stage, large-scale distortions of the lamellae are continuing and the rate is several times larger for the periodic boundary condition.

For the local equilibrium boundary condition, we may say that the system reaches the equilibrium at the late stage ($t \geqslant 500$), because there is no major difference between Fig. 3(c) ($t=500$) and Fig. 3(d) ($t=1000$). The time difference between (c) and (d) is comparable to the relaxation time scale τ, which can be estimated as follows. For $t \geqslant 500$, we may say that $H(t)$ decays exponentially. Using the values $H(500) \simeq 3.5 \times 10^{-10}$ and $H(1000) \simeq 8.7 \times 10^{-11}$, τ is estimated as $\tau \simeq 500/\ln[H(500)/H(1000)] \simeq 360$.

We also checked how the order parameter is equilibrated near the boundary. Shown in Fig. 4 is the order parameter change $\phi_2(t=1000) - \phi_2(t=0)$ in the adjacent sites (in the third outermost layer of the lattice). We can see that the boundary values are not frozen although its change is small compared to the change in the center of the bulk.

We also varied γ, the initial angle between the AB-rich lamellae and the phase boundary. In Fig. 5 shown are the snapshots taken at $t=1000$ for (a) $\gamma=40°$ with q_{1x} and q_{2x} having different signs and (b) $\gamma=90°$. In both cases, we see that the lamellae are sharply bent near the phase boundary. The bent is so sharp that the curve has an overshoot. In Fig. 5(a), the lamellae in the both phases exhibit undulation. In Fig. 5(b), only the long-chain lamellae are bent while the short-chain lamellae remain straight. This should be due to the difference in bending stiffness of the two phases. These morphologies are considered to be far from true equilibrium. However, we note that overshoots like in Fig. 5(a) have been

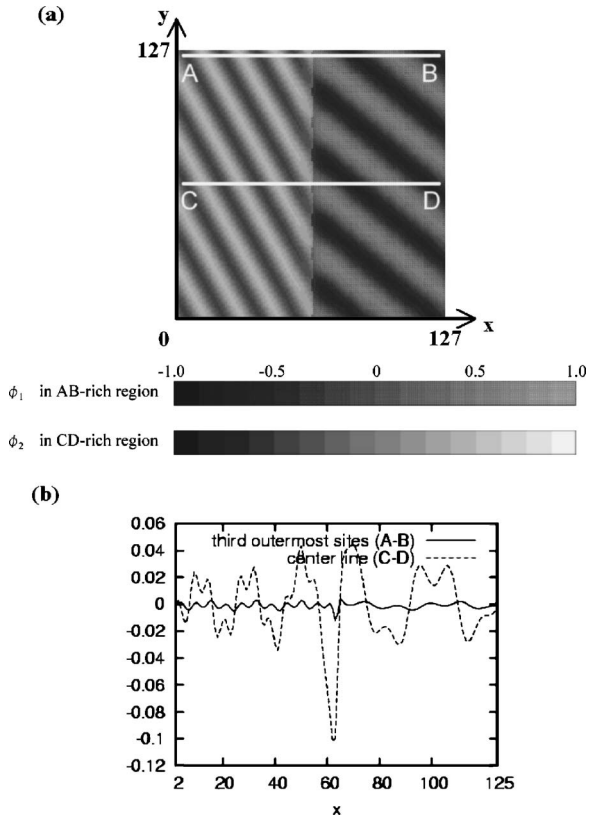

FIG. 4. (a) Snapshot at $t=1000$ with the local equilibrium boundary condition [same as Fig. 2(d) in the left-hand column]. (b) Change of order parameter $\phi_2(t=1000) - \phi_2(t=0)$ along cross sections A-B (third outermost sites) and C-D (center line) in panel (a).

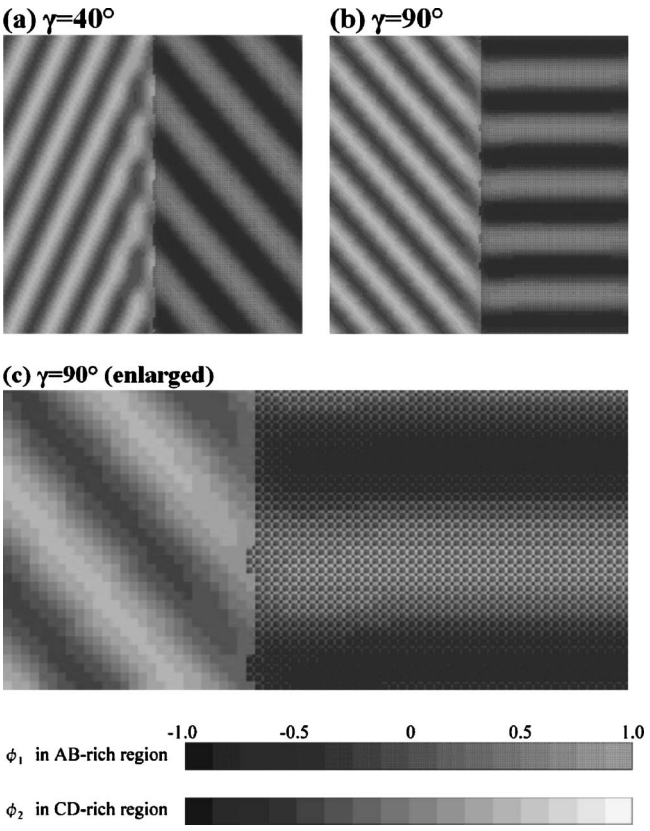

FIG. 5. Domain morphology for initial conditions with a large angle between the *AB* and *CD* lamellae. Snapshots at $t=1000$ obtained with the local equilibrium boundary condition. The angle γ is (a) 40° with q_{1x} and q_{2x} having the different sign, (b) 90°. (c) Magnified picture of the enclosed area of (b), which shows an "overshoot" in the wider stripe close to the phase boundary.

observed experimentally [see Fig. 4(a) of Ref. [12]]. To remove the irregular structure, we must rotate the whole lamellae. Such global motion does not occur in a realistic time scale in laboratories.

V. SUMMARY

In this paper, we introduced the local equilibrium boundary condition to minimize the effect of system size and to obtain equilibrium patterns for a bulk system. The method can be applied to a wide class of Ginzburg-Landau free energy and is especially advantageous for incommensurate systems. We applied it to the coexisting lamellar phases in a binary mixture of block copolymers. We showed that the new scheme leads to a more homogeneous pattern than the periodic boundary condition. By varying the initial angle between the two lamellae, we obtained overshoots of lamellar domains, which has been observed experimentally. These results support the advantage of the new boundary condition over conventional ones.

ACKNOWLEDGMENTS

The authors thank Professor Toshihiro Kawakatsu and Professor Helmut Brand for useful discussions and comments.

APPENDIX: INITIAL CONDITION

Here we explain the details of our initial condition. First we consider a single lamellar phase. We assume the order parameter profile

$$\phi_0(\mathbf{r}) = \phi_{00},$$

$$\phi_1(\mathbf{r}) = \phi_{10}\cos(\mathbf{q}\cdot\mathbf{r}), \tag{A1}$$

$$\phi_2(\mathbf{r}) = \phi_{20}\cos(\mathbf{q}\cdot\mathbf{r}).$$

where $\phi_{10}, \phi_{20} \ll \phi_{00} \simeq 1$, which corresponds to the weak segregation regime in the microphase separation and strong segregation regime in the macrophase separation. Substituting into Eq. (12) and using the relation $\cosh(x) \simeq 1 + x^2/2 + x^4/24$ for $x \ll 1$, we can approximate the free energy density $f=f(q, \phi_{00}, \phi_{10}, \phi_{20})$ as

$$f \simeq \sum_{K=1,2} \left(\frac{1}{4} S_K(q, \phi_{00}) \phi_{K0}^2 + \frac{A_K}{32} \phi_{K0}^4 \right) - A_0 \ln(\cosh \phi_{00}) + \frac{1}{2}\phi_{00}^2 - B_0 \phi_{10}\phi_{20},$$

$$S_K(q, \phi_{00}) = 1 - A_K - B_K \phi_{00} + C_K q^2 + \frac{\alpha_K}{q^2}. \tag{A2}$$

We minimize this with respect to q to obtain the equilibrium wave number,

$$q_0 = \left(\frac{\alpha_1 \phi_{10}^2 + \alpha_2 \phi_{20}^2}{C_1 \phi_{10}^2 + C_2 \phi_{20}^2} \right)^{1/4}. \tag{A3}$$

The resulting free energy density $f_0=f(q_0)$ is then minimized with respect to ϕ_{00}, neglecting the small cubic terms proportional to B_1 and B_2, and finally minimized with respect to ϕ_{10} and ϕ_{20} restoring the cubic terms. Thus we have two sets of solutions,

$$(q, \phi_{00}, \phi_{10}, \phi_{20}) = \begin{cases} (q_1, \Phi_0, \Phi_1 + \Delta_1, \Phi_2 + \Delta_2), \\ (q_2, -\Phi_0, \Phi_1 - \Delta_1, \Phi_2 - \Delta_2), \end{cases} \tag{A4}$$

which correspond to the *AB*-rich lamellae and *CD*-rich lamellae, respectively.

[1] M. M. Doria, J. E. Gubernatis, and D. Rainer, Phys. Rev. B **41**, 6335 (1990).
[2] G. Gonnella, E. Orlandini, and J. M. Yeomans, Phys. Rev. Lett. **78**, 1695 (1997).
[3] T. Teramoto, A. Saeki, and F. Yonezawa, J. Phys. Soc. Jpn. **69**, 679 (2000).
[4] H. Morita, T. Kawakatsu, M. Doi, D. Yamaguchi, M. Takenaka, and T. Hashimoto, J. Phys. Soc. Jpn. **73**, 1371 (2004).
[5] H. C. Andersen, J. Chem. Phys. **72**, 2384 (1980).
[6] M. Parrinello and A. Rahman, Phys. Rev. Lett. **45**, 1196 (1980); J. Appl. Phys. **52**, 7182 (1981).
[7] M. R. Wilson and M. P. Allen, Mol. Phys. **80**, 277 (1993).
[8] A. J. Schultz, C. H. Hall, and J. Genzer, J. Chem. Phys. **117**, 10329 (2002).
[9] M. Murat, G. S. Grest, and K. Kremer, Macromolecules **32**, 595 (1999).
[10] S. M. Allen and J. W. Cahn, Acta Metall. **27**, 1085 (1979).
[11] Y. Oono and S. Puri, Phys. Rev. Lett. **58**, 836 (1987); S. Puri and Y. Oono, Phys. Rev. A **38**, 1542 (1988).
[12] T. Hashimoto, S. Koizumi, and H. Hasegawa, Macromolecules **27**, 1562 (1994).
[13] T. Ohta, M. Motoyama, and A. Ito, J. Phys.: Condens. Matter **8**, A65 (1996).